Master's Thesis

Sintering using a 2-D Monte Carlo model with diffusion algorithm

Hyesoo Belinda Chung

Department of Materials Science and Engineering

Graduate School of UNIST

2019

Sintering using a 2-D Monte Carlo model with diffusion algorithm

Hyesoo Belinda Chung

Department of Materials Science and Engineering

Graduate School of UNIST

Sintering using a 2-D Monte Carlo model with diffusion algorithm

A thesis/dissertation submitted to
the Graduate School of UNIST
in partial fulfillment of the
requirements for the degree of
Master of Science

Hyesoo Belinda Chung

12.21.2018
Approved by

Advisor
Sukbin Lee

Sintering using a 2-D Monte Carlo model with diffusion algorithm

Hyesoo Belinda Chung

This certifies that the thesis/dissertation of
Hyesoo Belinda Chung is approved

12.21.2018

signature

Advisor: Sukbin Lee

signature

Thesis Committee Member #1: Ki-Suk Lee

signature

Thesis Committee Member #2: Han Gi Chae

Abstract

A Monte Carlo Potts Model that simulates the evolution of pores and grains during sintering is proposed. Sintering starts with the formation of necks between powder particles, and ends with the elimination of isolated pores in a process called densification. Unlike earlier numerical and simulation studies where the densification is achieved only through pore annihilation, the proposed model incorporates the control over various diffusion paths for matter transport and accurately reproduces pore evolution kinetics during final stage sintering. As the first test case, binary crystals with various dimensions in which a periodic array of pores lie on the grain boundary were sintered. It was found that the model reproduced previously reported theoretical and simulation results. As the second test case, two particles with equal radius placed next to each other were sintered only by surface diffusion, demonstrating that neck growth and time display the theoretical relationship.

Keywords: Monte Carlo / sintering /pore evolution / coarsening

Contents

List of figures

List of tables

1. Introduction

Sintering is a treatment applied to metal or ceramic powders to form a compact with material properties favorable for industrial use. The benefits of sintering compared to traditional metal casting are various. One of them is that microstructure of the material can be more easily controlled and predicted.

Microstructure determines the physical properties of materials. Traditional sintering usually requires heat and pressure for powder particles to coalesce. In general, complete densification of the compact is difficult to obtain, so additives are used to help densification in industrial processes [1].

Sintering simulations and experiments have been conducted in order to elucidate the mechanisms that lead to sintering and densification [2-6]. This paper aims to demonstrate that computer simulation with a modified Monte Carlo Potts model can be used to simulate sintering and reproduce realistic microstructures.

Different simulation methods have been used for sintering: molecular dynamics, FEM, kinetic Monte Carlo, etc [7-11]. Unlike molecular dynamics and FEM, Monte Carlo is simple and requires comparatively little computational power to model mesoscale system, which makes it suitable for grain growth simulations [12]. Assuming sintering is a phenomenon mainly driven by diffusion, we modified the Monte Carlo Potts model to simulate the different types of diffusion involved in sintering. In order to verify that the proposed model is able to simulate sintering, we used two test cases. The first case involves the sintering of a pore placed on a grain boundary, and the second case coarsening of two round particles.

2. Theoretical Background

2.1 Sintering

2.1.1 Driving force for sintering

Thermodynamically, sintering is driven by free energy minimization because it occurs to decrease the total interface energy. For crystalline particles, the kinetics of sintering is controlled by diffusion mechanisms [1].

According to Fick's diffusion law, diffusion occurs due to the chemical potential gradient and matter move from region of high potential to a region of low potential. The chemical potential of an atom located in a flat surface is lower than that of an atom in a curved surface. Such difference exists because surface energy causes a pressure difference across a curved surface. In other words, the pressure applied by the curved surface increases the chemical potential of its constituents.

A curved surface thus have a tendency to become planar to reduce its chemical potential. When one mole of material is transferred from a flat surface to a spherical surface, the work done is equal to the change in chemical potential, Δμ. The work required is the surface energy γ_s times the corresponding surface area change. The volume change of the spherical particle for the transfer of dn atoms is equal to the atomic volume, Ω, times dn.

$$\mathrm{dV} = 4\pi R^2 dR = \Omega dn \tag{1}$$

$$\Delta\mu = 2\gamma_s \frac{d(surface\ area)}{dn} = \gamma_s \cdot 8\pi \mathrm{RdR} \frac{\Omega}{dV} \tag{2}$$

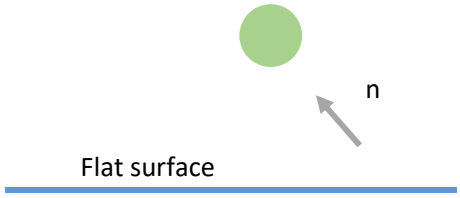

Figure 1. Transport of n atoms from a flat surface to the curved surface of a sphere

This work is equal to the change in surface energy. From such relationship the solubility or vapor pressure can be calculated, leading to the Thompson-Freundlich equation. According to the above equation, solubility is inversely proportional to the radius of the particle. Such relationship explains many phenomena found in nature. Sintering which involves small and large pores may also be affected by such phenomenon.

Interface energy which characterizes solid-solid, liquid-solid, and liquid-liquid boundaries is the energy required to form a unit area of new interface.

In solid state sintering, dihedral angles between particles are determined by the vapor-solid surface energy and solid-solid interface energy, which is the grain boundary energy. A balance of forces determines the dihedral angle by the following balance of forces.

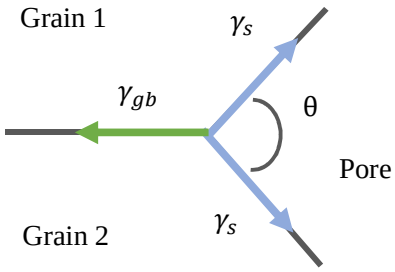

Figure 2. Dihedral angle where a grain boundary meets a pore

$$2\gamma_s cos\frac{\theta}{2} = \gamma_{gb} \quad (3)$$

$$\theta = 2\cos^{-1}\frac{\gamma_{gb}}{2\gamma_s} \quad (4)$$

In liquid phase sintering, solid-liquid interfaces and solid-solid interfaces are present and determine the equilibrium shape between particles and pores.

For a given dihedral angle, the curvature of the pore walls is determined by the number of grain boundaries intersecting the pore. If there are many grains surrounding a single pore, the walls are usually convex, otherwise they are concave. Concave walls with a positive stress usually shrink. Therefore, concave walls with high dihedral angles lead to easier pore removal.

This is why the size of powder compacts matters in sintering [13]. The larger the powder size is, the larger the pore size is. Densification occurs only when grains are larger than pores and the pore coordination number becomes small enough to facilitate shrinkage.

In terms of energy change, when a pore shrinks, surface energy decreases but grain boundary area increases. When the pore sides are concave to the pore, the increase in grain boundary energy is offset by the reduction in surface energy.

2.1.2. Mass transport paths in sintering

If we treat sintering as a thermodynamic phenomenon, each stage is driven by a different type of mass transport. There are several different mass transport paths involved in sintering: grain boundary diffusion, evaporation-condensation, surface diffusion, volume diffusion, and creep (plastic flow).

Surface diffusion and evaporation-condensation are usually considered as non-densifying mechanisms because they do not cause grain centers to get closer to one another. Meanwhile, grain boundary diffusion, vacancy diffusion and viscous flow are considered as densifying because they allow grain centers to get closer to one another. In sintering, densifying and non-densifying mechanisms compete against each other and the microstructure of sintered compacts reflect this competition of mass transport paths.

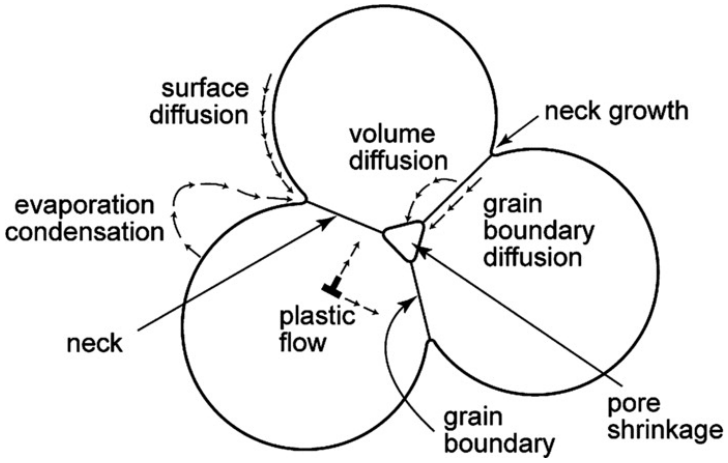

Figure 3. Mass transport paths in sintering [13]

The general atomic diffusion equation is

$$\mathrm{J} = \mathrm{C}\frac{D}{k_B T} \times \frac{d\mu}{da} \tag{5}$$

and volume change due to diffusion through an area A is

$$\frac{dV}{dt} = J \times A \times \Omega_o \tag{6}$$

where J is the species flux and Ω_o is the volume of the diffusing species [14]. When there is no shrinkage, the radius of the neck is approximately $\mathrm{r} \approx \frac{x^2}{2a}$ and the volume of the neck region is $\mathrm{V} = \int_0^x A dx \approx \pi\frac{x^4}{2a}$. If there is shrinkage, the radius of the neck is approximately $\mathrm{r} \approx \frac{x^2}{4a}$ and the volume of the neck region is $\mathrm{V} \approx \pi\frac{x^4}{4a}$.

Using the above diffusion equation and the volume formula, the neck growth rate and shrinkage rate in Table 1 can be derived for the initial stage of sintering

Table 1. Kinetic equations for sintering mechanisms of initial stage sintering [14].

Sintering Mechanism	Neck Growth	Shrinkage
Lattice diffusion from grain boundary to neck	$x^4 = \frac{16 D_l \gamma_s V_m a}{RT} t$	$\frac{\Delta l}{l} = \left(\frac{D_l \gamma_s V_m}{RT a^3}\right)^{1/2} t^{1/2}$
Grain boundary diffusion from grain boundary to neck	$x^6 = \frac{48 D_{gb} \delta_{gb} \gamma_s V_m a^2}{RT} t$	$\frac{\Delta l}{l} = \left(\frac{3 D_{gb} \delta_{gb} \gamma_s V_m}{4RT a^4}\right)^{1/3} t^{1/3}$
Viscous Flow	$x^2 = \frac{4\gamma_s a}{\eta} t$	$\frac{\Delta l}{l} = \frac{3\gamma_s}{8\eta a} t$
Surface Diffusion from particle surface to neck	$x^7 = \frac{56 D_s \gamma_s V_m a^3}{RT} t$	
Lattice diffusion from particle surface to neck	$x^5 = \frac{20 D_l \gamma_s V_m a^2}{RT} t$	
Evaporation-condensation from particle surface to neck	$x^3 = \sqrt{\frac{18}{\pi}} \frac{p_\infty \gamma_s}{d^2} \left(\frac{M}{RT}\right)^{3/2} at$	

2.1.3 Stages of sintering

Coble identified three stages of sintering: initial, intermediate, and final [15]. Initial stage is characterized by the formation of necks between powder particles and proceeds until pores form interconnected channels along three grain junctions. Also, during this stage, there is an increase of the particle contact area from 0 to 0.2 grain diameter and the relative density increases from 0.5 to 0.6.

During the intermediate stage, the pore channels become narrower and eventually undergo Rayleigh breakup, which forms discrete pores, and relative density increases from 0.6 to 0.9.

Then, in the final stage of sintering, the isolated pores are eliminated by mass transport from the grain boundary to the pore, and density increases up to 99%. Pores on grain boundaries are removed by grain boundary diffusion or lattice diffusion. While others within grains are eliminated by lattice diffusion only. Because lattice diffusivity is too slow, it is important for pores to remain attached to grain boundaries to reach full densification. Also, in polycrystals, grain growth takes place along with densification.

2.2 Earlier study of sintering

2.2.1 Pore Shrinkage Kinetics during final stage sintering

Hassold and Srolovitz proposed a Monte Carlo model for final stage sintering and verified their model by simulating the shrinking of pores placed on a grain boundary [16]. Their model simulated the kinetics of boundary migration, surface diffusion, and pore shrinkage, which occurs by grain-boundary diffusion only. The shrinkage probability in their model is

$$\mathrm{P} = \frac{D}{r\lambda} \tag{7}$$

where D is a scaling constant, r is the pore radius, and λ is the distance between pores.

When a vacancy site adjacent to a grain boundary is randomly selected, it executes a random walk along the grain-boundary path. If it reaches a pore by the end of the random walk, it is removed from the system. Otherwise, the vacancy site remains.

The initial size, shape and spacing of all the pores were identical. The ratio of surface to grain-boundary energy was set equal to unity, but the pore spacing and the ratio of grain boundary to surface diffusivity were varied. As shown in Figure 4, pores are completely removed from the system after 3 x 10^5 MCS.

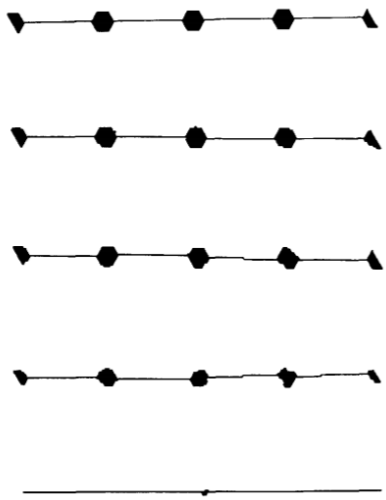

Figure 4. Time evolution of a periodic array of pores along a grain boundary [16].

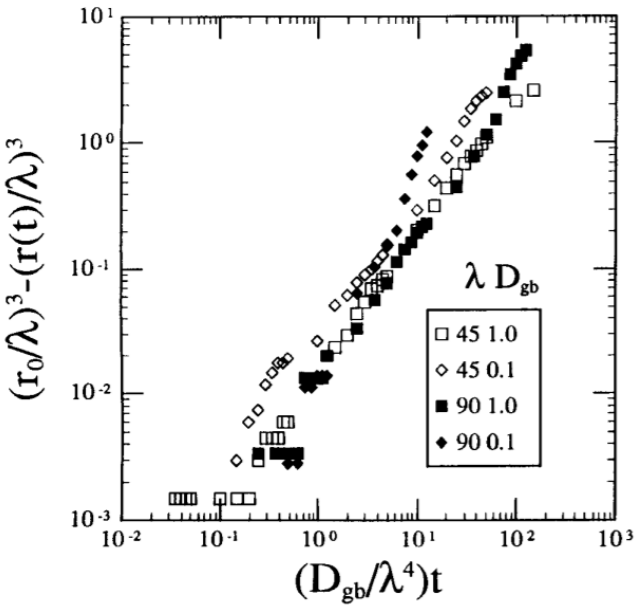

Figure 5. Normalized pore shrinkage kinetics for regular arrays of pores using different spacing and grain boundary diffusivity [16].

When they summarized their results, they observed that pore radius decreases with time as

$$r^3 = r(0)^3 - \frac{CD_{gb}t}{\lambda} \tag{8}$$

where C is a constant and r(0) is the initial pore size. Then, they normalized and plotted their data obtaining a straight line with a slope of unity shown. All the data cluster along the same straight line, but the line shifts to the left when D_{gb} becomes small.

2.2.2 Two-particle coarsening

Due to its simplicity, coarsening of two spherical particles has been studied and analyzed with different simulation tools[11,17]. Two particle coarsening is observed in the initial stage of sintering when matter fills the convex neck formed between two particles. There are a number of paths for material transport to the neck area in the initial stage. Evaporation-condensation and surface diffusion don't lead to densification but transfer material from the particle surface to the neck.

Calculating the vapor pressure over a neck of small negative radius is lower than that over a neck of large positive radius curvature. The difference in vapor pressure is approximately

$$\Delta p = \frac{p_0 \gamma V_m}{RT}\left(\frac{1}{\rho}\right) \tag{9}$$

where ρ is density, V_m is the molar volume and p_0 is the equilibrium vapor pressure over a flat surface. Setting the Langmuir adsorption equation with the approximated vapor pressure, the neck growth rate by evaporation-condensation is

$$\left(\frac{x}{r}\right)^3 = \left[\frac{3\sqrt{\pi}\gamma M^{3/2} p_0}{\sqrt{2}R^{3/2}T^{3/2}d^2}\right]\frac{t}{r^2} \tag{10}$$

In order to calculate neck growth through surface diffusion we use the equation for volume change of the neck due to diffusion through the neck area (6)

With only surface diffusion taking place, the volume change equation becomes

$$\frac{d}{dt}\left[\pi\frac{x^4}{2a}\right] = \frac{D_s}{RT} \times \frac{\gamma K}{L} \times 2\pi x 2\delta_s \times \Omega_0 \tag{12}$$

and the relationship between neck radius and time is derived

$$x^7 = \frac{56 D_s \gamma_s \delta_s a^3 \Omega_0}{RT} t \tag{13}$$

where x is the neck radius, a is the particle radius, D_s is the surface diffusion coefficient and δ_s is the diffusion thickness of the surface diffusion [14].

3. Monte Carlo model

3.1 Method

Monte Carlo Potts model is commonly used to simulate grain growth in polycrystals. Grains are composed of spins of the same number. Spins in the interior of a grain are surrounded by equal spins while spins at the grain boundary have at least one adjacent spin of different number. For grain growth simulation, a pair of adjacent spins is randomly selected and the Hamiltonian is calculated using the following equation:

$$H = \sum_{nn} \left(1 - \delta_{s_i s_j}\right) J(S_i S_j) \tag{14}$$

where S_i is the spin, and $\delta_{s_i s_j}$ is 1 when spins are same, and 0 when spins are different.

Then one of the spin is flipped, and the Hamiltonian of the new pair is calculated. If the energy of the new state is lower, the new state is accepted, otherwise, a random number is generated and compared with the Arrhenius equation.

Such algorithm can be modified for sintering simulation by classifying the different types of configurations and diffusion paths that a vacancy or a grain may take.

The proposed Monte Carlo Potts model selects a spin and determines whether the spin is a vacancy, a grain at the boundary, or a grain at a surface. Then, the energy state is calculated and either spin exchange or flip occurs depending on the type of configuration.

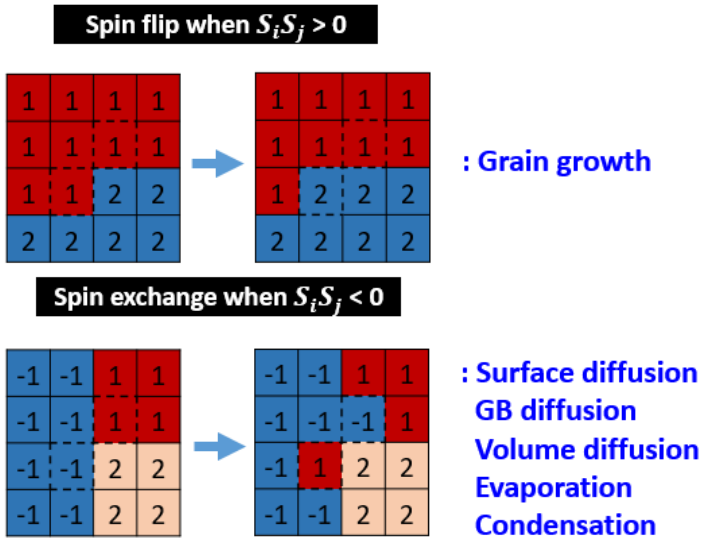

Figure 6. Condition for spin flip/exchange in the proposed model

If a pair of spins pertaining to different grains are selected, grain growth may occur through spin flip. If a vacancy and a grain are selected, spin exchange leading to the diffusion of vacancy may occur. The different types of diffusion rates are controlled by setting their success rates of diffusion. The modified model is supposed to simulate the different types of diffusions. Since sintering results from the complex interaction of vacancy and grains, theoretical and experimental research to identify the dominant type of diffusion and its rate has been conducted by earlier scholars

3.2 Parameters

Some parameters that determine the sintering rate in the model are the temperature, the diffusivity rates, and the surface/grain boundary energy ratio.
As temperature increases, probability of successful moves increases. The surface/grain boundary energy ratio determines the dihedral angle or the equilibrium shape between grains and pores.
The diffusivity rates that appear in the proposed model are as follows

- D_{gb} = grain boundary diffusion rate
- D_{hi} = interface diffusion rate
- D_{gbm} = grain boundary mobility rate
- D_{sdiss} = solid dissolution into bulk medium rate
- D_{mdiss} = vacancy dissolution into bulk solid rate
- D_{sprec} = solid precipitate onto any surface rate
- D_{mprec} = vacancy precipitate onto any surface rate

These diffusivity rates represent the success rate of each diffusion type, and their values are not comparable with the actual diffusivities of metals or ceramics.
In order to find the natural success rate of the grain boundary diffusivity rate and surface diffusivity rate, idealized systems where successful vacancy moves can be tracked are modeled and used to verify that the natural success rate increased or decreased with temperature.

4. Simulation & Results

4.1 Densification during final stage sintering

In order to verify that the proposed model works for sintering, sintering simulation similar to that of Hassold and Srolovitz was performed with the proposed Monte Carlo model.

In our system, pores of equal radius are placed on a grain boundary and they diffuse through the grain boundaries until they are removed from the grains. In order to compare the results with earlier work, the ratio of pore radius to inter-pore distance was set equal to that used in Hassold and Srolovitz's model, which is 1 to 7. Also, other parameters such as grain boundary mobility and grain boundary diffusivity are set close to 0 in order to suppress grain growth and allow only the diffusion pores in the simulation.

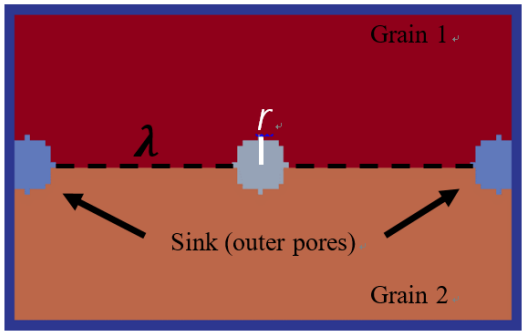

Figure 7. Initial setup of the simulation

First, a single pore whose spin is -1 is placed in the middle of a grain boundary between two grains as shown in Fig D. Then two pores with -2 spin are placed at each end of the grain boundary. The vacancy sites belonging to the middle pore whose spin is -1 diffuse through the grain boundary or through the bulk and attach to the pores located at each end of the grain boundary. On the other hand, grain boundary diffusion of pores whose spin are -2 is suppressed due to capillary effect and pressure difference. Therefore, the inner pore behaves as a source of vacancies, and the outer pores behave like sinks.

So, once a vacancy with -1 spin randomly diffuses through the grain boundary and reaches the outer pore, its spin switches to -2, which means it has been completely removed and become part of the outer

pore or void. The algorithm of the model also allows vacancy sites located at a triple junction to detach more easily from the pore with a modified Hamiltonian that includes surface energy in the equation

For the first test case, the ratio of pore radius to pore spacing was 9 and the grain boundary energy was 1.When the simulation was run, the middle pore retained its lens shape thanks to surface diffusion. With only grain boundary diffusion facilitated, the removal of all vacancy sites in a circular pore of radius 5 took approximately 20000 MCS.

For the second test case, the pore spacing was doubled. The pore shape did not evolve or shrink in a significantly different way from the previous case but computer time required to remove all vacancy sites from the grains increased dramatically. Such result was not surprising since each vacancy had to move through a longer grain boundary.

Then, similar simulations were run with different grain boundary diffusivities. When the grain boundary diffusion rate decreased from 1.0 to 0.5 and 0.1, sintering took much longer in MCS steps. This was an expected result, since the probability for a vacancy to exchange places with grains at the boundary decreased. Vacancies on the grain boundaries moved and left the system more slowly, while the pore maintained a smoother surface throughout the simulation. As the grain boundary diffusion rate decreased, vacancies at the pore surface had sufficient time to reach the equilibrium shape through surface diffusion.

After observing the evolution of pore shape, its size at each time step was measured and its radius was calculated assuming that it was a perfect circle. The result was used to plot the universal curve that Hassold and Srolovitz showed on his paper. With normalized time in the X-axis and normalized pore shrinkage in the Y-axis, a linear plot with slope close to unity was obtained as shown in Fig. 1

Shrinking does not start immediately in the proposed model, but it requires some incubation time for vacancies to move through the grain boundary before leaving the grains. Thus, the shrinking behavior does not look linear in the beginning. Also, when full densification is near, shrinking plateaus as the number of vacancies exiting decreases significantly. Therefore, after having 3 runs of the same system, initial data and final data were excluded from the analysis: only data pertaining to shrinkage above 15% and below 85% were considered.

Once the plots for each simulation were obtained, their slopes were calculated with linear fitting and the average was calculated as shown in Table 2.

Table 2. Average slope of the shrinkage curve for one pore array

	Egb = 0.1	Egb = 0.5	Egb = 1.0
λ = 45	0.83236	0.93553	0.8147
λ = 90	0.8638	0.93325	0.887

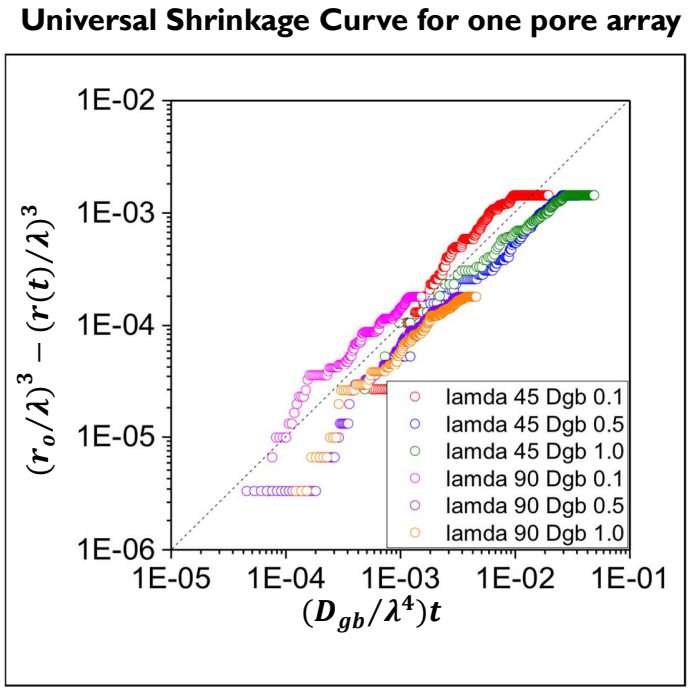

Figure 8. Normalized shrinkage plotted against normal time for different λ and different D_{gb}

Analyzing the curve when grain boundary diffusivity is 0.1, shrinking initiated much more quickly in this system where grain boundary diffusion rate was low. Such effect of grain boundary diffusivity on the system was also demonstrated in Hassold's and Srolovitz's work. They attributed the cause to the less complete equilibration of the pore shapes during densification when grain boundary diffusivity is high.

However, in our model, where grain boundary diffusivity is not directly affected by pore shape, the above explanation is not appropriate. With a higher rate of diffusivity, vacancies can switch places with grains more easily, but their movement is random: they can move either to the right or to the left. From the graph, we can deduce that the rate that vacancies escape from the grains does not have a perfectly

inverse relationship with grain boundary diffusivity. Therefore, what the shift in the universal curve means is that when grain boundary diffusivity increases, densification time does not decrease proportionally.

The one-pore-array shrinkage simulation proved that the proposed Monte Carlo Potts model is able to simulate the linear pore shrinkage kinetics during final stage sintering.

Then, other parameters such as the pore size and the number of pores were modified to observe if the model produced results consistent with previous works.

First, pore size was increased to see if there was any resolution effect. Two separate simulations with pores whose size are 5 and 10 respectively were run. Then, the evolution of pore shape was observed and the shrinkage curves were plotted. For the larger pore, total MCS to achieve complete shrinkage increased by more than ten times.

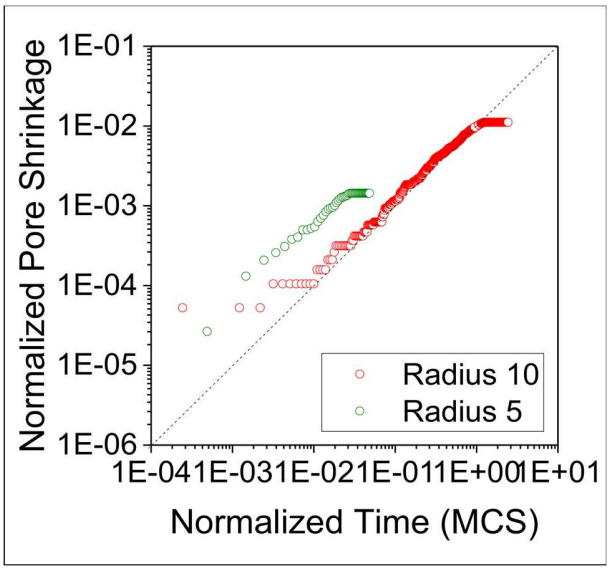

Figure 9. Shrinkage curves for two systems with different pore size

However, the larger the size, the more oval the shape of the pores remained throughout the process since vacancies were discretized and abnormal jumps that disturb the shape of the pore were less likely to happen. The overall linear behavior of each pore did not deviate significantly from theory.

For subsequent simulations with different grain boundary diffusion rates and different number of pores, a large system may require too much computational time and power, so pore radius size 5 was adopted.

Hassold's model had many pores placed on a grain boundary, and they all shrank at the same rate and at the same time. Whether their model is a realistic depiction of sintering is doubtful. If such case were realistic, the experiment conducted by Alexander and Balluffi with copper wires wouldn't show pores entrapped in the sintered microstructure [18].

So, what we did next with the proposed Monte Carlo model is to observe how pores shrink when there are more than one pore placed on a grain boundary. To observe the effect of the number of pores on the densification process, two, three, and four pores were placed on the grain boundary. The ratio of the pore radius to pore spacing was fixed, and the grain boundary diffusion rate was set 0.1.

Obviously, time for complete densification increased along with the number of pores placed on the grain boundary. Except for the increased time, the two-pore case showed similar behavior with the one-pore case. The two pores shrank almost at the same rate and, when the universal curve for the two-pore system was drawn, slope was close to unity as shown in Figure 10.

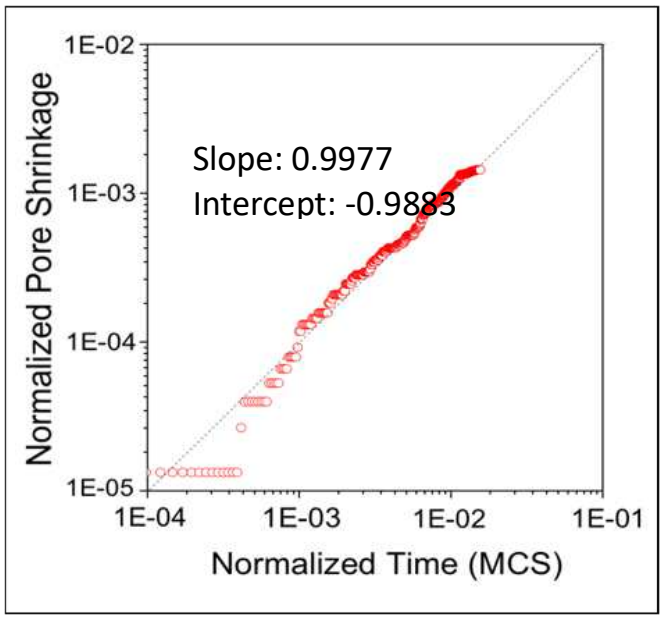

Figure 10. Pore shrinkage curve of a two-pore system with λ 45 and D_{gb} 0.1

Figure 11. Simulation snapshot of a two-pore system with λ 45 and D_{gb} 0.1

The three- and four-pore systems took even longer to reach full densification, and it was noteworthy that pores did not shrink in size uniformly. As shown in Fig. 12 and 14, pores shrank in size at their own pace, and some were removed from the system sooner than the others. Although the number of pores increased to three and four, vacancies could exit the system only through two paths while some vacancies left the pore only to attach to another. In other words, there was an exchange of vacancies between pores and this caused pores to grow or shrink non-simultaneously. While the general trend was the shrinking behavior of pores, temporary enlargement of pores could also be observed in some cases. When, the universal curves for the three-, and four-pore systems were drawn, their slope dropped below unity significantly.

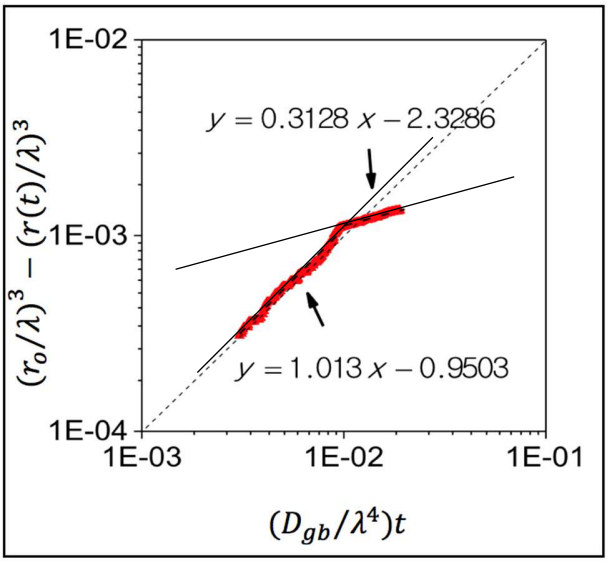

Figure 12. Pore shrinkage curve of a three-pore system with λ 45 and D_{gb} 0.1

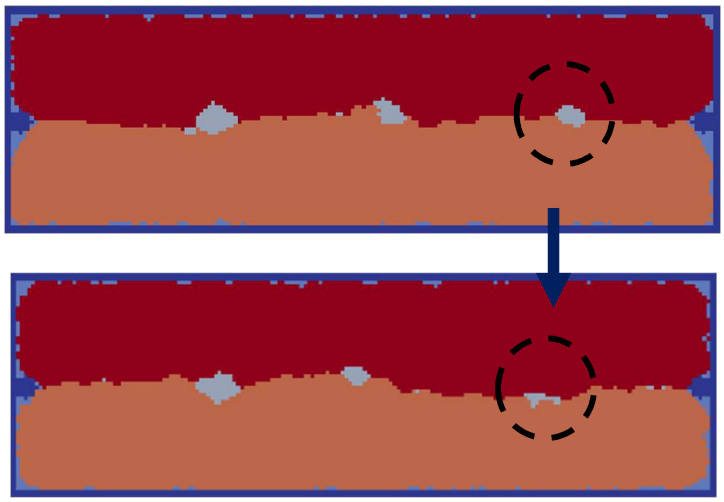

Figure 13. Simulation snapshots of pore shrinking in a three-pore system with λ 45 and D_{gb} 0.1

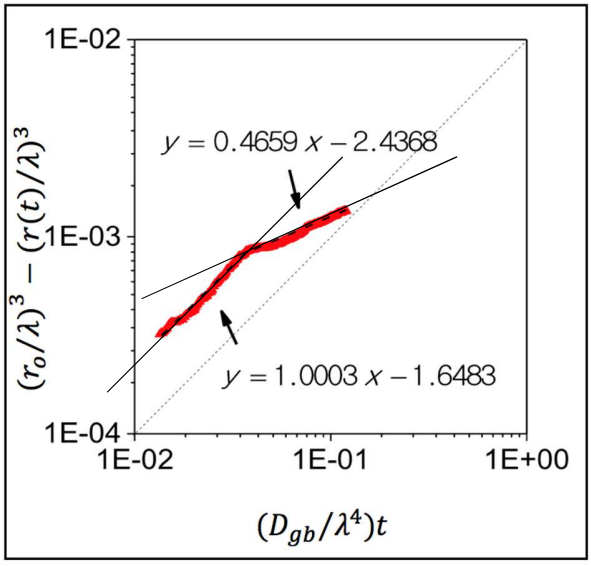

Figure 14. Pore shrinkage curve of a four-pore system with λ 45 and D_{gb} 1.0

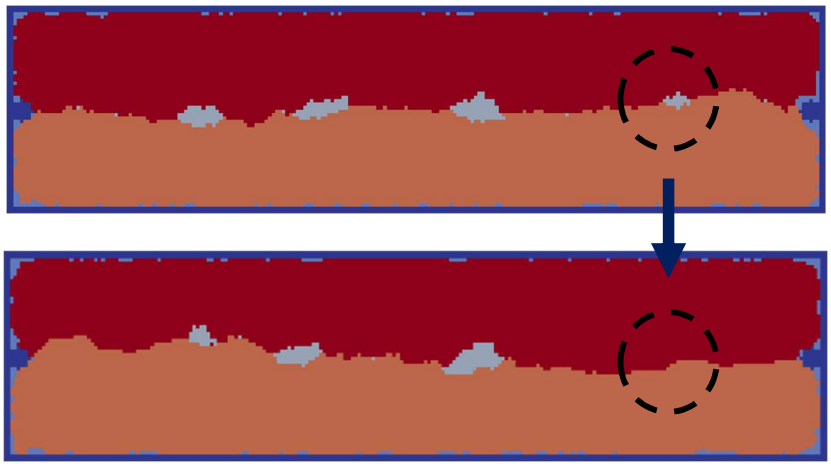

Figure 15. Simulation snapshots of pore shrinking in a four-pore system with λ 45 and D_{gb} 1.0

In short, the pore shrinkage kinetics for three- and four-pore cases was different from theory. With the interaction between pores, time to reach full densification took longer. In some cases, their pore shrinkage curves showed kinks, which indicated that shrinkage rate decreased significantly at certain points. Those time points were coincident with the complete removal of one of the pores from the system. When one of the pores is completely removed, the pore spacing, λ, is almost doubled, causing vacancies to travel longer distances to reach the sink. In short, such change in λ affects sintering time, and the shrinking curve no longer shows a linear curve.

4.2 Two-particle coarsening through surface diffusion

When two circular particles are placed next to each other barely touching, a small neck forms between them. Then, this neck grows and becomes the grain boundary between the two particles. Early sintering models approximated the neck saddle surface as a circle of diameter P as illustrated in Figure 15.

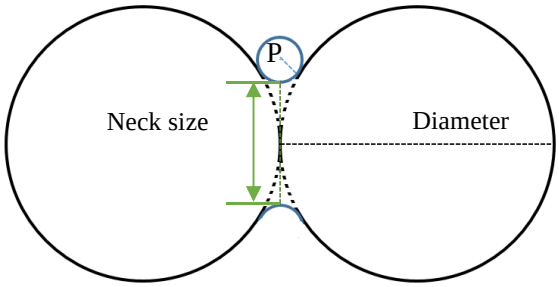

Figure 16. Neck geometry of two spheres in initial stage sintering

As neck grows, the solid-vapor surface area is annihilated while the solid-solid interface area increases. This phenomenon either happens by evaporation-condensation, and surface diffusion as described in section 3.2.2. The solid-solid grain boundary energy and solid-vapor surface energy are related by (3)

A limiting neck size X is set by the dihedral angle and the particle size D as follows:

$$X = D \sin\left(\frac{\emptyset}{2}\right) \tag{15}$$

As a result, materials with low grain boundary energy usually have a large limiting neck size X and sinter to full density.

With the proposed Monte Carlo model, initial stage sintering was simulated with two round particles of the same size.

Grain growth was suppressed by setting grain boundary mobility 0. Because there is no vacancy trapped between the two particles and moving across the grain boundary, the only mass transport mechanism that plays a role in neck growth is surface diffusion.

The grain boundary energy was set different to observe if the proposed Monte Carlo model was able to

reflect (15). Then, three systems with the ratio of grain boundary energy to surface energy set different from one another were simulated.

In real materials, grain boundary energy depends on the crystal misorientation across the boundary [1,14]. Therefore, in real crystals, grain boundary energy differs from grain side to grain side, but in our model, such anisotropy of grain boundary energy is neglected and only isotropic grain boundary energy is considered.

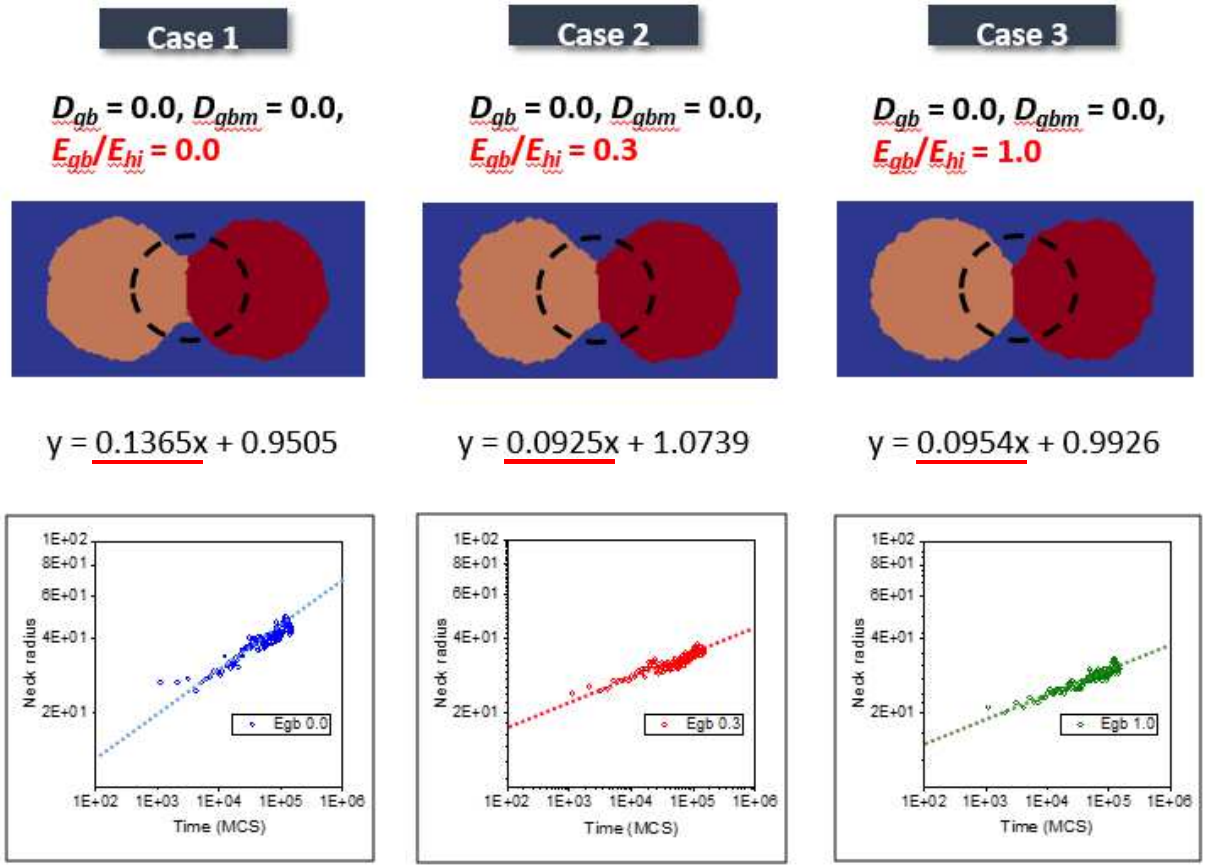

Figure 17. Neck growth in two-particle coarsening when E_{gb} is 0.0, 0.3, and1.0

After running 150000 MCS, the neck growth rate and particle shape of the particles were examined. The results of the simulation show that the dihedral angle between the two particles is wider and the

limiting neck size is larger when grain boundary energy is 0. Also, neck grows more slowly when grain boundary energy increases.

When we take the logarithm on both sides of equation (13), we obtain the following relationship between neck radius and time:

$$logr \sim 0.14logt + C \qquad (16)$$

where C is a constant.

In order to compare the results of the simulation with theory, neck radius measured at each time step was plotted against time in a log scale graph. Then the data were linearly fitted, and the slope of the linear fitting was compared to the slope in (16) for all three cases.

Consequently, we found that when grain boundary energy is set 0, the kinetics of the two particles is similar to the theoretical behavior. This is because equation (13) is derived by ignoring the effect of grain boundary energy and assuming surface diffusion is the only coarsening mechanism. Therefore, when grain boundary energy has a non-zero value, Monte Carlo model does not show the theoretical coarsening behavior illustrated by equation (13), but it does when the grain boundary energy is zero.

5. Conclusion

In this research, we developed a Monte Carlo Potts model that can simulate the different stages of sintering. Sintering is divided into three different stages: initial, intermediate, and final. In each stage, various mass transport mechanisms compete and the dominant mechanism can either lead to densification or coarsening of the powder compact.

In order to verify that the proposed Monte Carlo model is effective for sintering simulations, two well-supported cases were tested. One of them was the shrinkage of a pore array placed on a grain boundary and the other was the coarsening of two round particles. For the first case, the data obtained from the simulations were plotted and compared against the universal curve drawn by Hassold and Srolovitz. The result for the one-pore-array showed that the proposed Monte Carlo model successfully simulated vacancy diffusion through grain boundaries during final stage. For the second test case, neck growth between two particles was measured and the effect of grain boundary energy on the dihedral angle was analyzed. The results showed that the model could also reproduce coarsening by surface diffusion. Thus, the proposed Monte Carlo model was able to simulate both coarsening of two particles and pore evolution during final-stage sintering.

Further verification of the model could be performed by simulating the sintering of three particles in 2-D. Eventually, the proposed Monte Carlo model could be used to model the sintering of polycrystals and analyze the pore/grain distribution in sintered microstructures.

References

[1] Chiang, Y.; Birnie, D.; Kingery, W. *Physical ceramics*; Wiley: New York, 1997.

[2] Coble, R. *Journal of Applied Physics* 1961, *32*, 793-799.

[3] Kingery, W.; Berg, M. *Journal of Applied Physics* 1955, *26*, 1205-1212.

[4] Kuczynski, G. *Acta Metallurgica* 1956, *4*, 58-61.

[5] Burke, J. *Journal of the American Ceramic Society* 1957, *40*, 80-85.

[6] Okuma, G.; Kadowaki, D.; Hondo, T.; Tanaka, S.; Wakai, F. *Scientific Reports* 2017, *7*.

[7] Djohari, H.; Derby, J. *Chemical Engineering Science* 2009, *64*, 3810-3816.

[8] Djohari, H.; Martínez-Herrera, J.; Derby, J. *Chemical Engineering Science* 2009, *64*, 3799-3809.

[9] Tikare, V.; Braginsky, M.; Olevsky, E. *Journal of the American Ceramic Society* 2003, *86*, 49-53.

[10] Zeng, P.; Zajac, S.; Clapp, P.; Rifkin, J. *Materials Science and Engineering: A* 1998, *252*, 301-306.

[11] Zhang, W.; Schneibel, J. *Acta Metallurgica et Materialia* 1995, *43*, 4377-4386.

[12] Srolovitz, D.; Anderson, M.; Grest, G.; Sahni, P. *Scripta Metallurgica* 1983, *17*, 241-246.

[13] German, R. *Critical Reviews in Solid State and Materials Sciences* 2010, *35*, 263-305.

[14] Kang, S. *Sintering: Densification, Grain Growth and Microstructure*; Elsevier, 2004.

[15] Coble, R. *Journal of Applied Physics* 1961, *32*, 787-792.

[16] Hassold, G.; Chen, I.; Srolovitz, D. *Journal of the American Ceramic Society* 1990, *73*, 2857-2864.

[17] Wakai, F.; Yoshida, M.; Shinoda, Y.; Akatsu, T. *Acta Materialia* 2005, *53*, 1361-1371.

[18] Alexander, B.; Balluffi, R. *Acta Metallurgica* 1957, *5*, 666-677.

Acknowledgements

I would like to express my deep gratitude to Professor Sukbin Lee for his patient guidance, enthusiastic encouragement and useful critiques that have helped me grow as a person, student, and researcher.

I would also like to extend my thanks to my colleagues in the laboratory for their help in offering me the resources needed to conduct this research.